Bioconjugate Chemistry

Communication

pubs.acs.org/bc

Long-Term-Stable Near-Infrared Polymer Dots with Ultrasmall Size and Narrow-Band Emission for Imaging Tumor Vasculature *in Vivo*

Liqin Xiong,* Fengwen Cao, Xinmin Cao, Yixiao Guo, Yimin Zhang, and Xi Cai

School of Biomedical Engineering, Med-X Research Institute, Shanghai Jiao Tong University, Shanghai 200030, P. R. China

Supporting Information

ABSTRACT: Fluorescent nanoprobes have become one of the most promising classes of materials for cancer imaging. However, there remain many unresolved issues with respect to the understanding of their long-term colloidal stability and photostability in both biological systems and the environment. In this study, we report long-term-stable near-infrared (NIR) polymer dots for *in vivo* tumor vasculature imaging. NIR-emitting polymer dots were prepared by encapsulating an NIR dye, silicon 2,3-naphthalocyanine bis(trihexylsilyloxide) (NIR775), into a matrix of polymer dots, poly[2-methoxy-5-(2-ethylhexyloxy)-1,4-phenylenevinylene] (MEH-PPV), using a nanoscale precipitation method. The prepared NIR polymer dots were sub-5 nm in diameter, exhibited narrow-band NIR emission at 778 nm with a full width at half-maximum of 20 nm, and displayed a large Stokes shift (>300 nm) between the excitation and emission maxima. In addition, no significant uptake of the prepared NIR polymer dots by either human glioblastoma U87MG cells or human non-small cell lung carcinoma H1299 cells was detected. Moreover, these NIR polymer dots showed long-term colloidal stability and photostability in water at 4 °C for at least 9 months, and were able to image vasculature of xenografted U87MG tumors in living mice after intravenous injection. These results thus open new opportunities for the development of whole-body imaging of mice based on NIR polymer dots as fluorescent nanoprobes.

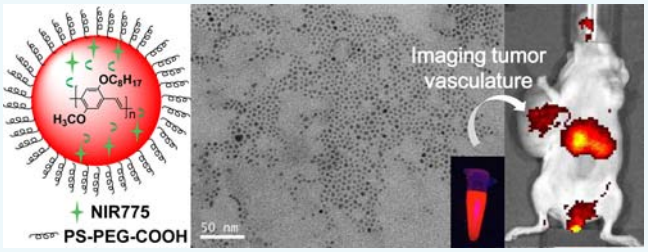

In recent years, conjugated polymer dots have gained interest as a new class of fluorescent probes due to their attractive chemical and optical features, such as bright fluorescence intensity, excellent photostability, high emission rates, and minimal cytotoxicity. Along with quantum dots, metal nanoclusters, carbon nanomaterials, up-conversion, and silicon nanomaterials, polymer dots are promising nanosized probes that have practical applications in biomedical research. Polymer dots have been demonstrated in various applications in bioimaging and biosensing.[1−11] The Chiu laboratory has developed fluorescent polymer dots for *in vitro* and *ex vivo* imaging.[12,13] We recently reported poly[2-methoxy-5-(2-ethylhexyloxy)-1,4-phenylenevinylene] (MEH-PPV) dots for *in vivo* lymph node imaging.[14] To date, only a few studies on whole-body imaging of polymer dots in living mice have been reported, mainly due to the challenges of designing polymer dots that show strong and narrow-band emissions in the near-infrared (NIR) region, and their unfavorable *in vivo* performance after systemic injection. Herein, for the first time, we report the synthesis of long-term-stable ultrasmall NIR-emitting polymer dots, which were successfully applied to whole-body tumor vasculature imaging of mice even 9 months after synthesis.

Smaller nanoprobes are often more desirable due to their favorable biodistribution characteristics in *in vivo* experiments.[15−18] Polymer dots prepared by nanoprecipitation are usually smaller compared to those prepared by a miniemulsion method and can be easily conjugated to biomolecules. We chose a nanoprecipitation method to prepare ultrasmall sub-5 nm polymer dots according to our previous work, with some modification.[14] Scheme 1 describes the synthesis of NIR polymer dots. An amphiphilic polymer, polystyrene-*graft*-ethylene oxide functionalized with carboxyl groups (PS-PEG-COOH),

Scheme 1. Chemical Structures of MEH-PPV, PS-PEG-COOH, and NIR775, Depicting the Preparation of NIR Polymer Dots[a]

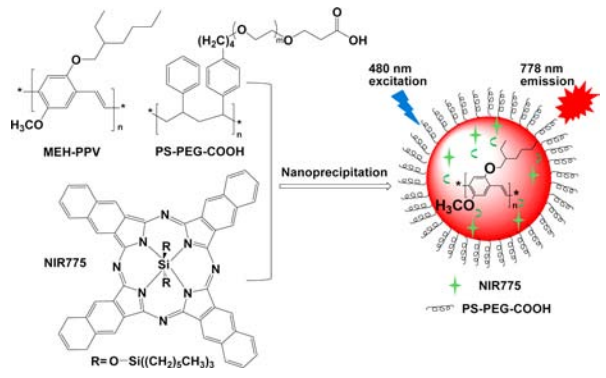

[a]The NIR emission is based on a FRET system utilizing NIR775 as an acceptor and MEH-PPV polymer as a donor.

Received: March 27, 2015
Revised: April 28, 2015
Published: April 30, 2015

DOI: 10.1021/acs.bioconjchem.5b00163
Bioconjugate Chem. 2015, 26, 817−821

was introduced to coat NIR polymer dots with a biocompatible shell. Narrow-band NIR emission was realized by doping the NIR dye, silicon 2,3-naphthalocyanine bis(trihexylsilyloxide) (NIR775), into the matrix of MEH-PPV dots.[14,19] To minimize the self-quenching effect among encapsulated NIR dyes and simultaneously get the highest fluorescence resonance energy transfer (FRET) efficiency, the optimal ratio of NIR775 to the MEH-PPV matrix (by weight) was found to be 0.012:1.

Transmission electron microscopy (TEM) shows that the NIR polymer dots were quite monodispersed, with an average diameter of 3.6 ± 0.4 nm (Figure 1, and Supporting Information,

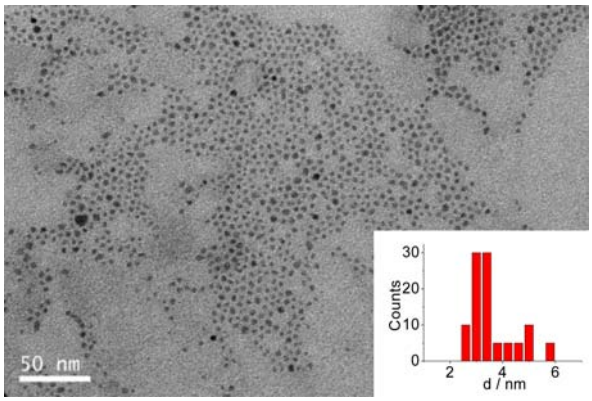

Figure 1. TEM image of the NIR polymer dots. Inset: average diameter of the NIR polymer dots obtained from the TEM result.

Figure S1). However, DLS data showed that the average hydrodynamic diameter of NIR polymer dots reached ~30 nm (Supporting Information, Figure S2), which was larger than the size determined by TEM. This increase in size is mainly due to the hydration corona formed by the PEG coating around NIR polymer dots. Further analysis revealed that the NIR polymer dots had a zeta potential of greater than −34 mV in water, indicating their good colloidal stability against aggregation (Supporting Information, Figure S3).

The MEH-PPV polymers in dilute THF solution exhibit a broad UV/vis band with a maximum at ~501 nm (Supporting Information, Figure S4). When the MEH-PPV chains are forced to densely pack into the nanoparticles by injecting the solution into an excess amount of water, the synthesized NIR polymer dots exhibit a broad UV/vis band with a maximum at 511 nm and a weak NIR peak at 773 nm (Figure 2). The appearance of this

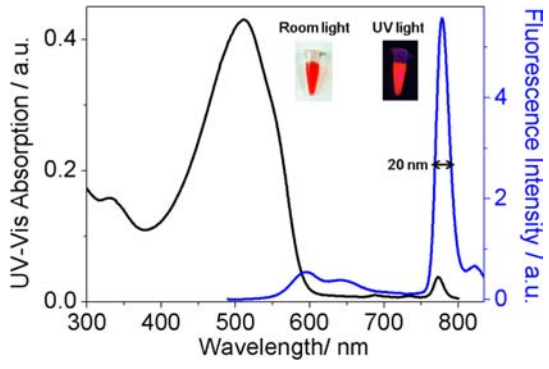

Figure 2. UV/vis absorption and fluorescence spectra of the NIR polymer dots. Insets are the room light and UV light photographs of the NIR polymer dots. The fluorescence photograph was obtained under 365 nm UV excitation, which showed red emission from the MEH-PPV.

red-shifted peak from 501 to 511 nm indicates the formation of inter- and/or intrachain aggregates where some conjugated segments or chromophores stack on top of each other. This result is consistent with previous studies reported by Traiphol.[20] Under excitation at 468 nm, these NIR polymer dots exhibited distinctive MEH-PPV emission at 595 nm with a shoulder at 644 nm, and a strong and narrow-band NIR peak at 778 nm with a full width at half-maximum (fwhm) as narrow as 20 nm. The absorbance and fluorescence spectra of NIR775 doped in MEH-PPV dots and dispersed in water were similar to the spectra of free NIR775 dyes dissolved in THF (Supporting Information, Figure S5). Conjugated polymers, such as MEH-PPV, are constructed of numerous fluorescent residues that form a large conjugated system and also exhibit very fast intra- and interchain photoexcitation transport (exciton diffusion). This structure allows the excitons to move along the polymer chain until they encounter a quencher molecule. This migration of excitons facilitates the FRET from the MEH-PPV polymer to the NIR775 dye over even relatively long distances. The amplified FRET process is further favored by the large extinction coefficient of NIR775 (5.2×10^5 M^{-1} cm^{-1}).[19] Additionally, the hydrophobic nature of NIR775 and the polymer dot matrix ensures close interaction between the acceptor dye and the donor matrix, which also enhanced efficient FRET. As a result, we observed highly efficient FRET despite the poor spectral overlap between MHE-PPV's fluorescence and NIR775's absorbance. The highest emission intensity ratio of 778 nm to 595 nm was over 10, confirming that efficient FRET occurred from the MEH-PPV matrix to NIR775 in the synthesized NIR polymer dots. We calculated the Förster radius (R_0) of the pair to be 3.5 nm. The quantum yield of the 778 nm emission (NIR775) from NIR polymer dots in water was about 0.09, slightly higher than that from the free NIR775 dyes in THF.[14] Furthermore, FRET resulted in a large Stokes shift (>300 nm) between the excitation and emission maxima, and thus can effectively reduce the high fluorescence background during *in vivo* imaging. These data demonstrate great potential of the synthesized polymer dots for NIR imaging.

We carried out a stability test of the NIR polymer dots in Tris buffer, HEPES buffer, PBS buffer, and Hanks's solution at 37 °C for 10 h each (Figure 3A). The results showed that the NIR polymer dots had the highest intensity in PBS; the fluorescent intensity in PBS was 1.32-fold higher than that in Tris buffer, 1.44-fold higher than that in HEPES buffer, and 1.16-fold higher than that in Hanks's solution. We then tested the temperature stability of the NIR polymer dots in PBS at 4, 22, and 37 °C for 45 h each (Figure 3B). As expected, the NIR polymer dots had the highest intensity at 4 °C; the fluorescent intensity at 4 °C was 1.30-fold higher compared with that at 22 °C, and 1.68-fold higher compared with that at 37 °C. We also tested the long-term stability of the NIR polymer dots at 4 °C: no aggregation was observed after storage in water at a concentration of 50 μg/mL for at least 9 months. These data further demonstrated excellent long-term stability against aggregation of the NIR polymer dots.

The cytotoxicity of the NIR polymer dots was evaluated by the CCK-8 assay in human glioblastoma U87MG cells and human non-small cell lung carcinoma H1299 cells. No differences in cell viability were observed in the absence or presence of the NIR polymer dots at a concentration of 5−100 μg/mL at 37 °C for 24 h (Figure 3C). These data confirmed that the NIR polymer dots exhibit negligible cytotoxicity.

To ascertain whether the NIR polymer dots were uptaken by live cells, we used a confocal microscope to examine the uptake of

DOI: 10.1021/acs.bioconjchem.5b00163
Bioconjugate Chem. 2015, 26, 817−821

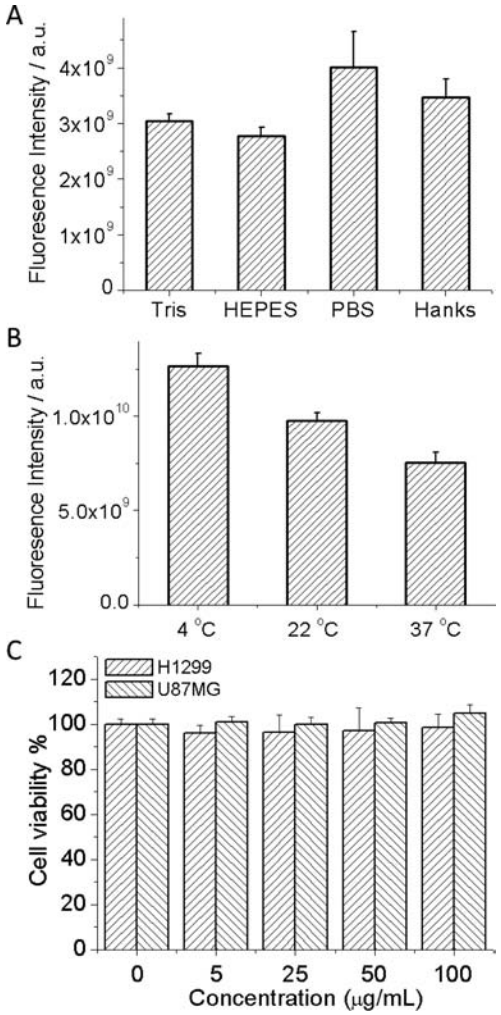

Figure 3. (A) Stability of the NIR polymer dots in Tris buffer, HEPES buffer, PBS buffer, and Hanks's solution at 37 °C for 10 h (about 1 μg of dots per sample). (B) Temperature stability of the NIR polymer dots in PBS for 45 h (about 3 μg of dots per sample). (C) Viability values (%) of cells estimated by CCK-8 assay versus incubation concentrations of the NIR polymer dots. Data represent mean ± SD (n = 3).

the NIR polymer dots in two cell lines, U87MG and H1299. After 6 h of incubation at a concentration of 10 μg/mL, nearly no NIR fluorescence signal was detected in both cell lines (Supporting Information, Figure S6). This is probably because of the large negative surface charges arising from the carboxyl groups. We further tested three NIR polymer dots samples with different surface charges, −34.4, −21.7, and −15.3 mV, which displayed fluorescence intensity similar to that of the background by flow cytometry analysis (Supporting Information, Figure S7). These data suggested that the NIR polymer dots were not taken up by either U87MG cells or H1299 cells.

For *in vivo* imaging, we used the NIR polymer dots synthesized and stored at 4 °C up to 9 months. Athymic nude mice (n = 3) were administered the NIR polymer dots (~50 μg per mouse) through tail-vein injection. At 24 h post injection, the mice were imaged using an IVIS spectrum imaging system with a 465 ± 15 nm excitation filter and a 780 ± 10 nm emission filter. Intense NIR fluorescence signal was observed in the liver, bladder, and lymph nodes (Supporting Information, Figure S8). Ultrasmall sub-5.5 nm particles were reported to pass through the barrier for renal clearance, and nanoparticles with sizes ranging from 10 to 200 nm show very high distributions in the liver and spleen due to reticuloendothelial system absorption.[21−29] The detected NIR fluorescence signal in the liver and bladder suggested the existence of both ultrasmall and large NIR polymer dots. Furthermore, these NIR polymer dots showed lower uptake in the lymph nodes compared with the lager polymer dots.[14] This is because the size of nanoparticles exhibits a strong effect on the migration time during lymph node mapping, and the nanoparticles with a hydrodynamic diameter of 30−50 nm were reported to exhibit long-time and high uptake into the lymphatic system.[14,30,31]

For *in vivo* tumor imaging, the NIR polymer dots (~25 μg per mouse) stored after 3, 6, and 9 months were then injected intravenously into nude mice bearing a U87MG tumor on the left shoulder (stomach position). Thirty minutes post injection, a strong NIR fluorescence signal was clearly observed in the U87MG tumor vasculature of the mice (Figure 4, Supporting

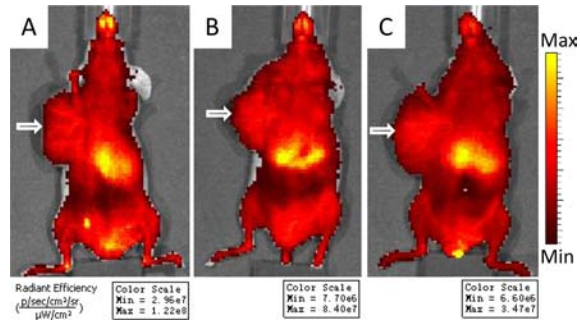

Figure 4. *In vivo* fluorescence imaging of U87MG tumor-bearing mice (n = 6, tumors are indicated by white arrows). (A) 30 min post injection NIR polymer dots prepared after 3 months, (B) 30 min post injection NIR polymer dots prepared after 6 months, and (C) 60 min post injection NIR polymer dots prepared after 9 months (excitation filter, 465 ± 15 nm; emission filter, 780 ± 10 nm).

Information, Figure S9). It is very interesting to observe that the prepared NIR polymer dots were not taken up by live U87MG cells *in vitro* but accumulated in the U87MG tumor *in vivo*. It is probably because tumor tissue vasculatures are leaking and hyperpermeable, allowing preferential accumulation of nanoparticles in the tumor vasculature and tumor interstitial space (called passive nanoparticle tumor targeting). In particular, no obvious fluorescence intensity changes were detected among the three mice (Figure 4), indicating excellent long-term photostability of the NIR polymer dots. Region of interest (ROI) measurements (Supporting Information, Table S1) showed that the tumor-to-liver signal intensity ratios in three mice were 0.76, 0.73, and 0.72, respectively. The tumor-to-skin signal intensity ratios were 1.26, 1.49, and 1.77, respectively, and the tumor-to-background signal intensity ratios were 28.78, 19.13, and 19.21, respectively. The increase in the tumor fluorescence signal in mice was further obtained 20 h post injection (Table S1). These data demonstrated successful imaging of U87MG tumor in living mice by using the NIR polymer dots. However, under the same experimental conditions, nearly no fluorescence signal was visualized in the H1299 tumor of the mice injected with the NIR polymer dots (Supporting Information, Figure S10). The difference observed between these two tumor types is likely due to the different tumor microenvironments.

In conclusion, we prepared the NIR-emitting polymer dots by encapsulating the dye NIR775 into the matrix of MEH-PPV dots using a nanoprecipitation method. The synthesized NIR polymer

DOI: 10.1021/acs.bioconjchem.5b00163
Bioconjugate Chem. 2015, 26, 817−821

dots showed ultrasmall sub-5 nm size, exhibited narrow-band NIR emission at 778 nm with a fwhm of 20 nm, and displayed a large Stokes shift (>300 nm) of the emission maxima. In addition, no significant uptake of the synthesized NIR polymer dots by either U87MG cells or H1299 cells was observed. Furthermore, these NIR polymer dots exhibited long-term colloidal stability and photostability in water at 4 °C for at least 9 months, and were successfully applied to imaging vasculature of U87MG tumors in living mice after intravenous injection. To the best of our knowledge, this is the first successful demonstration of ultrasmall NIR polymer dots for *in vivo* tumor imaging. This study provides a foundation for the development of whole-body tumor imaging based on the use of polymer dots as fluorescent nanoprobes.

■ ASSOCIATED CONTENT

Supporting Information

Experimental details, TEM, DLS, zeta potential, absorption and fluorescence spectra, cell imaging, flow cytometric histogram, fluorescence images of mice, and ROI measurements. The Supporting Information is available free of charge on the ACS Publications website at DOI: 10.1021/acs.bioconjchem.5b00163.

■ AUTHOR INFORMATION

Corresponding Author

*E-mail: xiongliqin@sjtu.edu.cn.

Notes

The authors declare no competing financial interest.

■ ACKNOWLEDGMENTS

This work was supported by grants from the Chinese Natural Science Foundation project (no. 81301261, no. 21374059), the Shanghai Pujiang Project (no. 13PJ1405000), and Doctoral Fund of Ministry of Education of China (no. 20130073120098).

■ REFERENCES

(1) Pecher, J., and Mecking, S. (2010) Nanoparticles of conjugated polymers. *Chem. Rev. 110*, 6260−6279.

(2) Wu, C. F., and Chiu, D. T. (2013) Highly fluorescent semiconducting polymer dots for biology and medicine. *Angew. Chem., Int. Ed. 52*, 3086−3109.

(3) Zhu, C. L., Liu, L. B., Yang, Q., Lv, F. T., and Wang, S. (2012) Water-soluble conjugated polymers for imaging, diagnosis, and therapy. *Chem. Rev. 112*, 4687−4735.

(4) Pu, K. Y., Shuhendler, A. J., Valta, M. P., Cui, L., Saar, M., Peehl, D. M., and Rao, J. H. (2014) Phosphorylcholine-coated semiconducting polymer nanoparticles as rapid and efficient labeling agents for in vivo cell tracking. *Adv. Healthcare Mater. 3*, 1292−1298.

(5) Sun, W., Hayden, S., Jin, Y. H., Rong, Y., Yu, J. B., Ye, F. M., Chan, Y. H., Zeigler, M., Wu, C. F., and Chiu, D. T. (2012) A versatile method for generating semiconducting polymer dot nanocomposites. *Nanoscale 4*, 7246−7249.

(6) Wei, L., Zhou, P., Yang, Q. X., Yang, Q. Y., Ma, M., Chen, B., and Xiao, L. H. (2014) Fabrication of bright and small size semiconducting polymer nanoparticles for cellular labelling and single particle tracking. *Nanoscale 6*, 11351−11358.

(7) Wu, C. F., Bull, B., Szymanski, C., Christensen, K., and McNeill, J. (2008) Multicolor conjugated polymer dots for biological fluorescence imaging. *ACS Nano 2*, 2415−2423.

(8) Feng, G. X., Li, K., Liu, J., Ding, D., and Liu, B. (2014) Bright single-chain conjugated polymer dots embedded nanoparticles for long-term cell tracing and imaging. *Small 10*, 1212−1219.

(9) Kim, S., Lim, C. K., Na, J., Lee, Y. D., Kim, K., Choi, K., Leary, J. F., and Kwon, I. C. (2010) Conjugated polymer nanoparticles for biomedical in vivo imaging. *Chem. Commun. 46*, 1617−1619.

(10) Wagh, A., Qian, S. Y., and Law, B. (2012) Development of biocompatible polymeric nanoparticles for in vivo NIR and FRET imaging. *Bioconjugate Chem. 23*, 981−992.

(11) Chan, Y. H., Wu, C., Ye, F., Jin, Y., Smith, P. B., and Chiu, D. T. (2011) Development of ultrabright semiconducting polymer dots for ratiometric pH sensing. *Anal. Chem. 83*, 1448−1455.

(12) Wu, C. F., Schneider, T., Zeigler, M., Yu, J. B., Schiro, P. G., Burnham, D. R., McNeill, J. D., and Chiu, D. T. (2010) Bioconjugation of ultrabright semiconducting polymer dots for specific cellular targeting. *J. Am. Chem. Soc. 132*, 15410−15417.

(13) Wu, C. F., Hansen, S. J., Hou, Q., Yu, J. B., Zeigler, M., Jin, Y. H., Burnham, D. R., McNeill, J. D., Olson, J. M., and Chiu, D. T. (2011) Design of highly emissive polymer dot bioconjugates for in vivo tumor targeting. *Angew. Chem., Int. Ed. 50*, 3430−3434.

(14) Xiong, L. Q., Shuhendler, A. J., and Rao, J. H. (2012) Self-luminescing BRET-FRET near-infrared dots for in vivo lymph-node mapping and tumour imaging. *Nat. Commun. 3*, 1193.

(15) Tallury, P., Kar, S., Bamrungsap, S., Huang, Y. F., Tan, W., and Santra, S. (2009) Ultra-small water-dispersible fluorescent chitosan nanoparticles: synthesis, characterization and specific targeting. *Chem. Commun. 17*, 2347−2349.

(16) Phillips, E., Penate-Medina, O., Zanzonico, P. B., Carvajal, R. D., Mohan, P., Ye, Y. P., Humm, J., Gonen, M., Kalaigian, H., Schoder, H., Strauss, H. W., Larson, S. M., Wiesner, U., and Bradbury, M. S. (2014) Clinical translation of an ultrasmall inorganic optical-PET imaging nanoparticle probe. *Sci. Transl. Med. 6*, 260ra149/1−10.

(17) Zhou, C., Long, M., Qin, Y. P., Sun, X. K., and Zheng, J. (2011) Luminescent gold nanoparticles with efficient renal clearance. *Angew. Chem., Int. Ed. 50*, 3168−3172.

(18) Li, Z., Sun, Q., Zhu, Y. A., Tan, B. E., Xu, Z. P., and Dou, S. X. (2014) Ultra-small fluorescent inorganic nanoparticles for bioimaging. *J. Mater. Chem. B: Mater. Biol. Med. 2*, 2793−2818.

(19) Jin, Y. H., Ye, F. M., Zeigler, M., Wu, C. F., and Chiu, D. T. (2011) Near-infrared fluorescent dye-doped semiconducting polymer dots. *ACS Nano 5*, 1468−1475.

(20) Traiphol, R., and Potai, R. (2013) Controlling chain organization and photophysical properties of conjugated polymer nanoparticles prepared by reprecipitation method: The effect of initial solvent. *J. Colloid Interface Sci. 403*, 58−66.

(21) Longmire, M., Choyke, P. L., and Kobayashi, H. (2008) Clearance properties of nano-sized particles and molecules as imaging agents: Considerations and caveats. *Nanomedicine 3*, 703−717.

(22) Alric, C., Miladi, I., Kryza, D., Taleb, J., Lux, F., Bazzi, R., Billotey, C., Janier, M., Perriat, P., Roux, S., and Tillement, O. (2013) The biodistribution of gold nanoparticles designed for renal clearance. *Nanoscale 5*, 5930−5939.

(23) Xiong, L. Q., Chen, Z. G., Yu, M. X., Li, F. Y., Liu, C., and Huang, C. H. (2009) Synthesis, characterization, and in vivo targeted imaging of amine-functionalized rare-earth up-converting nanophosphors. *Biomaterials 30*, 5592−5600.

(24) Xiong, L. Q., Yang, T. S., Yang, Y., Xu, C. J., and Li, F. Y. (2010) Long-term in vivo biodistribution imaging and toxicity of polyacrylic acid-coated upconversion nanophosphors. *Biomaterials 31*, 7078−7085.

(25) Xiong, L. Q., Chen, Z. G., Tian, Q. W., Cao, T. Y., Xu, C. J., and Li, F. Y. (2009) High contrast upconversion luminescence targeted imaging in vivo using peptide-labeled nanophosphors. *Anal. Chem. 81*, 8687−8694.

(26) Yang, L., Kuang, H. J., Zhang, W. Y., Aguilar, Z. P., Xiong, Y. H., Lai, W. H., Xu, H. Y., and Wei, H. (2015) Size dependent biodistribution and toxicokinetics of iron oxide magnetic nanoparticles in mice. *Nanoscale 7*, 625−636.

(27) Hirn, S., Semmler-Behnke, M., Schleh, C., Wenk, A., Lipka, J., Schaeffler, M., Takenaka, S., Moeller, W., Schmid, G., Simon, U., and Kreyling, W. G. (2011) Particle size-dependent and surface charge-dependent biodistribution of gold nanoparticles after intravenous administration. *Eur. J. Pharm. Biopharm. 77*, 407−416.

(28) Zheng, J., Zhou, C., Yu, M. X., and Liu, J. B. (2012) Different sized luminescent gold nanoparticles. *Nanoscale 4*, 4073−4083.

DOI: 10.1021/acs.bioconjchem.5b00163
Bioconjugate Chem. 2015, 26, 817−821

(29) Liu, J. B., Yu, M. X., Zhou, C., Yang, S. Y., Ning, X. H., and Zheng, J. (2013) Passive tumor targeting of renal-clearable luminescent gold nanoparticles: long tumor retention and fast normal tissue clearance. *J. Am. Chem. Soc. 135*, 4978−4981.
(30) Noh, Y. W., Kong, S. H., Choi, D. Y., Park, H. S., Yang, H. K., Lee, H. J., Kim, H. C., Kang, K. W., Sung, M. H., and Lim, Y. T. (2012) Near-infrared emitting polymer nanogels for efficient sentinel lymph node mapping. *ACS Nano 6*, 7820−7831.
(31) Xiong, L. Q., Shen, B., Behera, D., Gambhir, S. S., Chin, F. T., and Rao, J. H. (2013) Synthesis of ligand-functionalized water-soluble $[^{18}F]YF_3$ nanoparticles for PET imaging. *Nanoscale 5*, 3253−3256.

DOI: 10.1021/acs.bioconjchem.5b00163
Bioconjugate Chem. 2015, 26, 817−821